REPORT DOCUMENTATION PAGE

Form Approved
OMB No. 0704-0188

1. REPORT DATE *(DD-MM-YYYY)*	**2. REPORT TYPE**	**3. DATES COVERED** *(From - To)*
2/1/2012	Final Report	1 April, 2009 - 30 November 2011

4. TITLE AND SUBTITLE

Laser Diagnostics Study of Plasma Assisted Combustion for Scramjet Applications

5a. CONTRACT NUMBER

5b. GRANT NUMBER
FA9550-09-1-0282

5c. PROGRAM ELEMENT NUMBER

6. AUTHOR(S)

Tonghun Lee

5d. PROJECT NUMBER

5e. TASK NUMBER

5f. WORK UNIT NUMBER

7. PERFORMING ORGANIZATION NAME(S) AND ADDRESS(ES)

Tonghun Lee
2555 Engineering Building, Department of Mechanical Engineering
Michigan State University, East Lansing 48824-1226

8. PERFORMING ORGANIZATION REPORT NUMBER

9. SPONSORING / MONITORING AGENCY NAME(S) AND ADDRESS(ES)

Energy Conversion & Combustion Sciences Program (PM: Chiping Li)
Air Force Office of Scientific Research
875 North Randolph Street
Arlington VA 22203-1768

10. SPONSOR/MONITOR'S ACRONYM(S)

AFOSR

11. SPONSOR/MONITOR'S REPORT NUMBER(S)

AFRL-OSR-VA-TR-2012-0529

12. DISTRIBUTION / AVAILABILITY STATEMENT

Approved for public release; distribution is limited

13. SUPPLEMENTARY NOTES

none

14. ABSTRACT

The main goal of this study is to apply advanced laser imaging and optical diagnostics to study the physicochemical impact of nonequilibrium plasmas to enhance the conversion of chemical energy in combustion, and to investigate new efficient concepts for coupling plasma energy into a flame, seeking future potential application in high speed engines including scramjets. Three separate topics have been investigated within the scope of this objective. The first topic involves quantitative planar laser-induced fluorescence (PLIF) imaging of nitric oxide (NO) in a transient arc DC plasmatron torch using premixed air/fuel mixtures.The second topic is the investigation of a novel concept of coupling the plasma energy directly into the reaction zone of the combustion (Direct Coupling).The final topic involves the study of 'direct plasma coupled' flames in more practical geometries for both premixed and non-premixed conditions.

15. SUBJECT TERMS

Plasma assisted combustion, laser diagnostics, direct coupling, microwave plasma

16. SECURITY CLASSIFICATION OF:			**17. LIMITATION OF ABSTRACT**	**18. NUMBER OF PAGES**	**19a. NAME OF RESPONSIBLE PERSON**
a. REPORT	**b. ABSTRACT**	**c. THIS PAGE**			Chiping Li
U	U	U	UU	30	**19b. TELEPHONE NUMBER** *(include area code)* 703-481-6930

Standard Form 298 (Rev. 8-98)
Prescribed by ANSI Std. Z39.18

Final Report

LASER DIAGNOSTICS STUDY OF PLASMA ASSISTED COMBUSTION FOR SCRAMJET APPLICATIONS

AFOSR Grant Number: FA9550-09-1-0282
Period of Research: 04/01/2009 to 11/30/2011

Submitted to:

The Air Force Office of Scientific Research
Energy Conversion and Combustion Sciences
Program Manager: Dr. Chiping Li

Submitted by:

Tonghun Lee
Associate Professor
Department of Mechanical Engineering
Michigan State University
2555 Engineering Building
East Lansing MI 48824-1226

December 2011

TABLE OF CONTENTS

1 ABSTRACT

The main goal of this study is to apply advanced laser imaging and optical diagnostics to study the physicochemical impact of nonequilibrium plasmas to enhance the conversion of chemical energy in combustion, and to investigate new efficient concepts for coupling plasma energy into a flame, seeking future potential application in high speed engines including scramjets. Three separate topics have been investigated within the scope of this objective.

The ***first topic involves quantitative planar laser-induced fluorescence (PLIF) imaging of nitric oxide (NO) in a transient arc DC plasmatron*** torch using premixed air/fuel mixtures. Measurements of NO were made over a wide range of flow conditions and input plasma power levels. The concentrations in the imaging field were quantified using a multi-line calibration method involving spectroscopic modeling of NO LIF. Results show that NO formation in the igniter with high to moderate plasma energy coupling in a flame is considerable higher than that predicted by normal thermal mechanisms, but still an order of magnitude lower than cases where a plasma discharge is present without a flame. In addition to the NO imaging, flame dynamics for premixed and non-premixed configurations in the DC plasmatron were also investigated. The ***second topic is the investigation of a novel concept of coupling the plasma energy directly into the reaction zone of the combustion (Direct Coupling).*** An atmospheric high-Q re-entrant cavity applicator is used to couple microwave (2.45GHz) electromagnetic energy directly into the reaction zone of a premixed laminar methane-oxygen flame for flame enhancement, where ionization of the reaction zone is achieved with power levels as low as 6 W. PLIF imaging of OH and CO are conducted in the reaction zone over this transition, as well as spectrally resolved flame emission measurements to monitor excited state species and determine temperature conditions. Re-ignition conditions for the plasma discharge are also examined. The ***final topic involves the study of 'direct plasma coupled' flames in more practical geometries for both premixed and non-premixed conditions***. For this study, a new waveguide based high-Q microwave torch was developed to couple microwave fields directly into the reaction zone. OH number densities and temperature fields were measured using PLIF and Rayleigh scattering, respectively. In all conditions, increases in OH radical density and temperature as functions of power are observed. For the non-premixed flame, plasma energy is mostly coupled into the air first in terms of heat, which appears to be the main mechanism for flame holding with final flame temperatures exceeding 3000 K. Premixed flames where a fuel rich mixture injected directly into the plasma region showed significant improvement in flame stability where effects of non-thermal kinetic and fuel reforming effects were dominant.

2 INTRODUCTION

Advanced supersonic and hypersonic propulsion systems such as the scramjets will be key components of high-speed transportation for both military and civilian applications in the future. The combustion process in these engines typically involves highly turbulent reactive flow conditions, often beyond the limits of our physicochemical understanding. This study will provide a transformative advancement in our knowledge of highly turbulent flame dynamics over a wide range of conditions relevant to next generation propulsion systems. The United States Air Force devotes significant effort in fundamental research as well as development of advanced prototypes such as the X-51 scramjet shown in Figure 1, and this study will provide a foundational scientific knowledge base to further these efforts.

Figure 1. X-51 scramjet prototype (United States Air Force, 2010).

Development of next generation propulsion systems is fraught with a vast range of technical challenges. The scramjet for example, which offers the benefits of a simple design, reduced weight, low drag and high combustion efficiency, also faces significant technical challenges in flow control and combustion stability due to the supersonic airflow through the entire engine and resulting high Reynolds number regimes [1-2]. In case of hypersonic scramjet engines, upstream influences do not propagate within the free stream of the combustion chamber. As a result, throttle control at the entrance of the thrust nozzle is ineffective and a block of gas entering the combustion chamber must mix sufficiently with the fuel and undergo combustion before the burned gas is expanded through the nozzle. This limits the temperature and pressure ranges which allow efficient fuel-air mixing and stable combustion to occur. Operation outside this range can result in various acoustic problems, oscillations and instabilities in the combustion due to the mutual coupling between the unsteady heat release and local flow fluctuations in the flame zone [3]. Therefore, flame stabilization is one of the major issues to be addressed in the continued development of hypersonic propulsion systems in the future. In general, flame holding is achieved by three techniques: (1) organization of a recirculation area where the fuel and air can be partially mixed at low velocities, (2) interaction of a shock wave with partially or fully mixed fuel and oxidizer, and (3) formation of coherent structures containing unmixed fuel and air, wherein a diffusion flame occurs as the gases are convected downstream [4]. Recently, the use of a non-equilibrium plasma discharge has emerged as a promising means of achieving both ignition and combustion stability in hypersonic propulsion systems [5], where the generation of increased ions and electrons in the plasma discharge accelerate and enhance the chemical reactions involved in combustion.

Plasma Enhanced Combustion

The advantages of combining electromagnetic radiation with thermal oxidation include faster and more intense chemical energy conversion [6], increased stability in the lean flammability limit [7], reduction of pollution by altering oxidation byproducts, improved fuel efficiency

through more complete combustion [8,9], more reliable and rapid ignition [10], and stable fuel oxidation across a broader range of pressures and temperatures.

Previous studies in plasma enhanced combustion have examined: pre-treatment of the fuel or reactants into hydrogen rich syngas prior to thermal oxidation [11-12], enhanced ignition of hydrocarbon fuels [9,13-14], increased stability of combustion at atmospheric pressure [7,15-17], changes in chemical conversion efficiency [18], stabilization of diffusion flames [15,19-20], and enhanced combustion stability for supersonic propulsion systems [5,10]. Non-equilibrium plasmas [21-25] offer a particular effective solution where energy transfer occurs to specific pathways, which accelerate the flame chemistry without excessive deposition of heat. In comparison, thermal plasmas (*i.e.*, arc, spark, *etc.*) rely mainly on heat as the means of enhancing the combustion chemistry. A survey of the plasma enhanced combustion literature reveals that plasma impacts hydrocarbon chemistry through: (1) rapid decomposition of the fuel into smaller hydrocarbon molecules by chemically active species [26], (2) radiation-induced electron excitation [10], (3) localized ohmic heating which increases the rates of reaction and transport, and in-situ fuel reforming [26]. Recently, chemically excited species such as oxygen, $O_2(a^1\Delta_g)$, have been shown to increase flame speeds [27], and computational chemical kinetic models with integrated hydrocarbon and plasma reactions have been compared with measurements made in the laboratory test rigs [28-31].

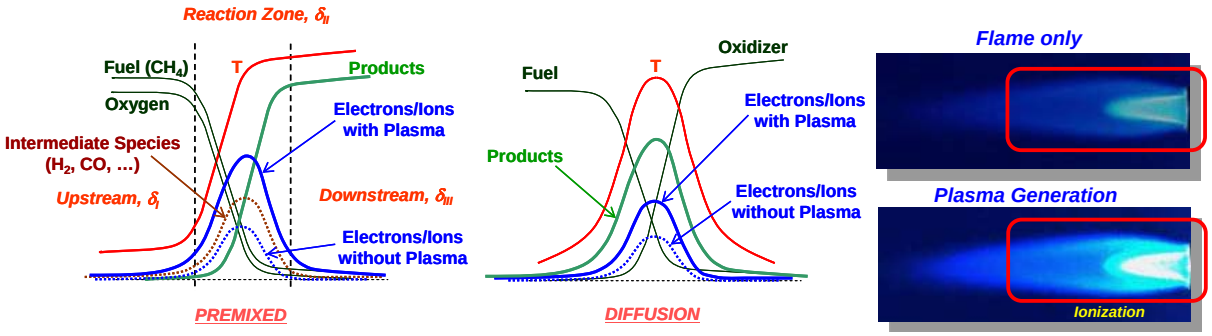

Figure 2. Direction coupling of plasma energy to the reaction zone of the flame. Left figure illustrates change in electron and ion concentrations in the reaction zone. Right figure shows a picture of a premixed flame with and without plasma energy coupling.

Direct Plasma Coupling

Over the past three years at Michigan State University, the concept of direct plasma coupling has been actively investigated, which is at the core of this report. Direct coupling refers to a method where the high electromagnetic field which generates the plasma is superimposed directly into the reaction zone of the flame as shown in Figure 2. As the flame itself already has electrons at high temperatures, the plasma energy is coupled into the flame chemistry with relative ease and is able to ionize the combustion species to enhance the radical chemistry. The concept was demonstrated in a dimensionally simple entrant cavity microwave plasma discharge system [32-33], where ionization of a small premixed flame was achieved with powers as low as 6 W. A more detailed description will follow in section 4.

Impact on Air Force Mission

The current research is expected to have a significant impact on the development of advanced supersonic and hypersonic airbreathing propulsion systems in the Air Force, as well as

contribute to enhancement of combustion research in general. The progress outlined here has been carried out in collaboration with the Propulsion Directorate of Wright Patterson Air Force Base to ensure that the objectives of the study are in line with future research targets of the Air Force. The results have confirmed the feasibility of a direct coupled plasma enhanced combustor which can be used for flame stabilization in advanced combustion prototypes of the future beyond the conventional limitations of the status quo.

It is expected that the basic research proposed here will be integrated into existing hypersonic propulsion research programs at the Air Force such as the successor to the X-51. The ability to enhance combustion stability, flame speed, and exothermic oxidation characteristics will offer the potential to design more flexible and robust hypersonic airbreathing propulsion systems capable of operating over a wide range of temperature and pressures, and at the very limits of high altitude and high velocity flight. Ultimately, the diagnostic capabilities will help to speed up the realization of hypersonic scramjets as a practical propulsion system for the Air Force and help maintain the dominance of the U.S. in the global aerospace arena.

3 PLASMA ENHANCED FLAMES IN A TRANSIENT ARC DC PLASMATRON

Nitric Oxide Imaging in a Transient Arc DC Plasmtron

In this study, we investigated nitric oxide formation in a premixed flame in a DC arc plasmatron with high-level plasma energy coupling using planar laser-induced fluorescence (PLIF). In plasma assisted combustion, analysis of the NO formation mechanism becomes difficult to determine as energy distribution of individual molecules can deviate from thermal equilibrium and the relationship between the NO production and deposition of heat is unclear. More importantly, high electron density generated by the electric field gives rise to new electron and ion impact processes which can enhance the propagation and branching of radicals and ultimately accelerate NO production. As NO formation is a major concern for all practical combustion systems, it is important to understand what the behavior of NO formation is in a plasma coupled flame, as plasmas can drastically alter nitrogen reaction pathways.

The main goal of this study was to present and demonstrate quantitative 2-D imaging of nitric oxide (NO) concentrations in the reaction zone of a transient arc plasmatron igniter over a wide range of operating conditions using planar laser-induced fluorescence imaging. In so doing, the focus was on determining the main pathways for NO formation as well as potentially using the NO itself as a tracer for investigation of the plasma and flame interaction. Additionally, the NO generated in these flame holding discharges can influence the overall chemistry of the main combustor itself, particularly when the NO levels are sufficiently high.

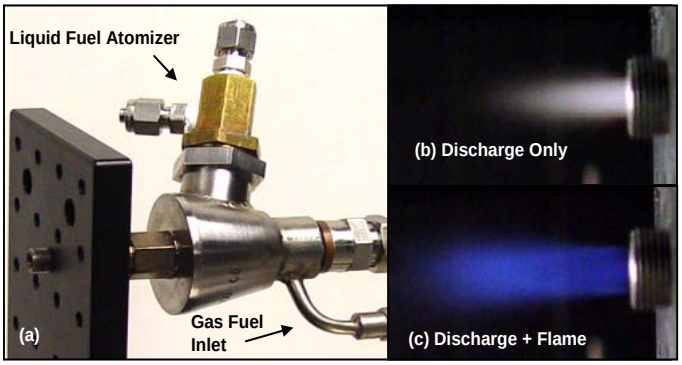

Figure 3. Imaging and schematic of transient arc plasmatron (a); Air plasma imaging at 20 SCFH and 300 mA (b); Plasma assisted stoichiometric methane/air imaging at 20 SCFH and 300 mA (c).

The plasma igniter in this work, shown in Figure 3, is a transient direct current (DC) discharge system based on the high voltage arc plasmatron [23,34-36]. The transient arc DC system operates on a repetitive glow to spark transition mode, offering the advantages of a thermal plasmatron with low average power output and temperature (T_g < 1200 K in air plasma, $n_e \sim 10^{14\text{-}15}$ cm^{-3}). During glow to spark transition (~100 ns), a short duration spark or diffused channel arises. The torch works mainly in the glow mode with voltage applied to the cathode (inner electrode) and the surrounding anode. One advantage is that the electrode erosion is less problematic than traditional DC torches due to the lower electrode temperature. Therefore, intensive cooling is not required. Classical DC arc plasmatrons operate using very high current while this new plasma igniter/plasmatron uses a semi-glow discharge with random complete or incomplete transitions to spark which results in highly efficient ignition and flame control with relatively low current, and thus low average power. This spark exists for only about 100 nanosecond, also hence termed as being ‘transient’. The spark is established inside the chamber inner walls and the main electrode (cathode) in the center of the chamber. It is noted that this does not expose the full interaction of the plasma and flame chemistry, and only the main reaction zone of the flame is available for optical diagnostics. This deficiency is fully addressed in our microwave plasma research, which follows after this section.

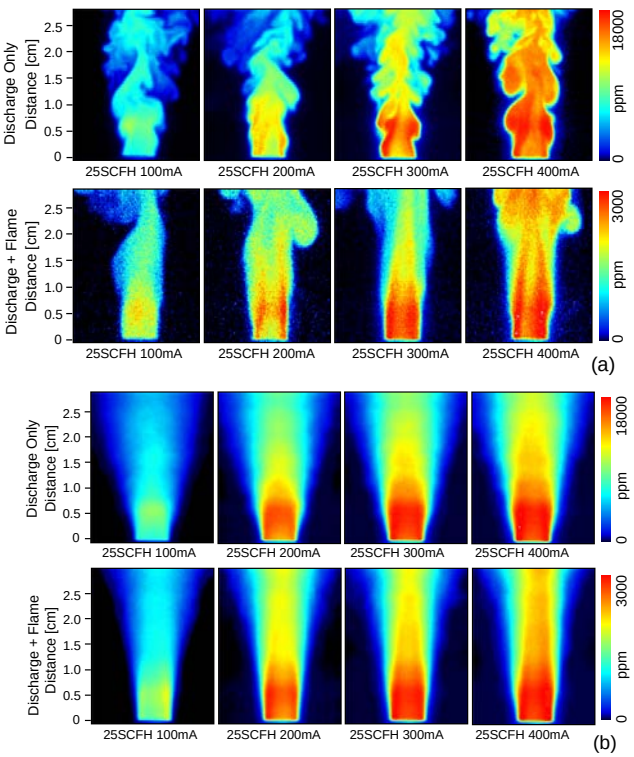

Figure 4. Single shot NO concentration fields using NO PLIF of gas discharge of air and plasma enhanced flames with different plasma power at same gas flow rate (a). Averaged NO concentration fields from NO PLIF of plasma enhanced flames with different plasma power at same gas flow rate (b).

The excitation of NO using $A_2\Sigma^+ - X_2\Pi$ (0,0) transition requires narrowband UV light near 226 nm, which was achieve by pumping a dye laser with the third harmonic (355 nm) from a 10 Hz Nd:YAG laser. Quantitative concentration of NO is calibrated by comparing the LIF signal to a well defined flat-flame calibration torch and using a NO addition method. Quantitative measurements of NO as a function of gas flow rate (20 to 50 SCFH), plasma power (100 to 900 mA, 150 to 750 watt) and equivalent ratio (0.7 to 1.3) are shown in Figure 4. NO production in a DC plasmatron can be significantly high near the reaction zone and that the glow to spark transition strongly affects the NO production via increase in the electron density. NO occurs predominantly through $N_2(v)+O \rightarrow NO+N$ for the plasma only case without combustion. The NO concentration for the plasma coupled combustion case (500 to 3500 ppm) was an order of magnitude less than the plasma discharge only case (8000 to 15000 ppm) due to the reduction of NO from the hydrocarbon chemistry. This result is mainly due to the fact that much of the plasma energy is now consumed by fuel reforming reactions and the resulting C_1 and C_2 radicals consume much of the oxygen as well as quenching the electron impact reactions which can drastically increase the NO formation in a plasma only discharge.

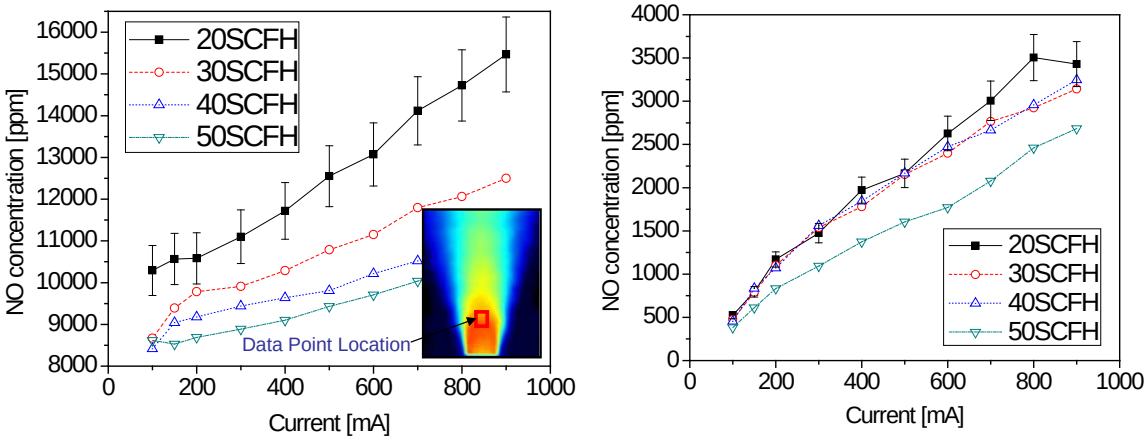

Figure 5. Nitric oxide concentrations in the reaction zone of the flame for plasma only case with air (left), and plasma with combustion (right). Methane and air flame is used at ϕ=1 for various flowrates.

Figure 5 shows the quantified NO concentrations in the reaction zone of the flame for

various flowrates both with and without combustion in a plasma discharge as a function of power. It is clearly shown here that the NO formation with a flame results in an order of magnitude less nitric oxide than just the plasma only case. Another reason for this phenomenon is the reverse Zeldovich reactions which lead to dissociation of the NO molecule when the hydrocarbon chemistry is coupled with the plasma. The NO generation is the highest for lower flow rates as concentration of energy per molecule is drastically increased. The concentrations presented here were calibrated for temperature effects by using a highly sensitive multi-line spectral fitting technique, which was previous established by funding also through AFOSR funding. Further details regarding this study can be found at [37].

Transient Arc DC Plasmatron: Premixed and non-premixed flames

In this study, efforts were made to study the impact of plasma on flame structure, chemical species production (OH and CO), and energy efficiency for premixed and non-premixed flame configurations in the transient arc DC plasmatron. From a practical perspective, the geometry of the plasma discharge and the flame is also a critical parameter that influences both chemistry and the flow dynamics of the system, and other commercial prototype systems have used both configurations. A quasi non-equilibrium plasma discharge from a transient-arc DC plasmatron is used over a wide range of flowrates and input powers to stabilize a methane-air flame. The plasma and flame interaction can drastically change depending on the relative location of the reaction zone and discharge, resulting in varying degrees of thermal and non-equilibrium effects for combustion enhancement. By understanding the impact of the plasma discharge for these configurations, we can deduce optimized design guidelines for a new generation of practical plasma enhanced combustion systems with higher efficiency and increased combustion stability.

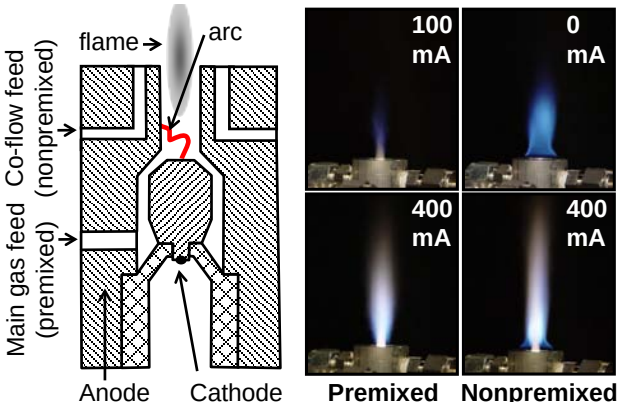

Figure 6. Schematic of transient arc plasmatron with cathode in the center and two different inlets are used to get two different experimental setup (left); Images for premixed (100 mA and 400 mA DC current) and nonpremixed (0 and 400 mA DC current) flames of methane/air with equivalence ratio of 0.9.

The discharge system used in this study is a modified version of the transient arc direct current (DC) plasmatron to accommodate both premixed and non-premixed flame geometries. There are two gas inlets in this discharge system: a lower one is connected directly to the arc chamber, and a top inlet provides co-flow around the main exit of the torch, as shown in Figure 6. In the premixed mode, a mixture of fuel and air flows through the lower inlet, while a nitrogen co-flow is sent through the top inlet to further stabilize the flame and cut off entrainment of atmospheric oxygen. In the *non-premixed mode*, air flows through the lower inlet (to generate the discharge) and methane through the top inlet. As this is an igniter for a combustor, it is designed for high flow with plasma stabilization. Therefore, most of the flowrates used in this study are conditions that are too high for unassisted stabilization; however, a few low power non-premixed mode settings where natural stabilization can be achieved are also employed, as shown in Figure 6 (upper right figure).

In order to visualize the region of rapid radical propagation, hydroxyl (OH) radical LIF imaging was carried out. Single and ensemble averaged OH Planar Laser-Induced Fluorescence (PLIF) images are shown in Figure 7 as a function of increasing microwave power for both premixed (top) and nonpremixed flames (bottom). Average images were based on acquisition of 200 instantaneous images. Here, the total flow rate for the reactants is 9 standard liters-per-minute (LPM, referenced to STP conditions), and the equivalence ratio is ϕ=0.95. The equivalence ratio in the nonpremixed case is defined here as the ratio between the fuel and oxygen in the inner nozzle. At these conditions, combustion power from the oxidation of the fuel is about ~500 W using the lower heating value of methane. For first order comparisons showing rough magnitude and trend, measurements using a thermocouple show that temperatures for premixed flames are about 100 to 200 K higher than that in non-premixed flames for the same fuel flowrates. For premixed flames, the visible flame luminosity and plasma volume increase with increased current/power. The range for current is 100 to 900 mA in our current research, resulting discharge power of 150 to 750 Watts. At low powers (~100 mA), the OH signal is lower than in a typical premixed flame, presumably because a significant portion of the oxidation reactions occur inside the arc chamber, where the mixture initially comes in contact with the discharge. When the DC current is higher, the reaction rates are expected to increase, resulting in a more compact flame structure especially as a larger portion of the fuel is oxidized inside the chamber. However, the introduction of added species and charged particles with more momentum (and new reaction chemistry involving ions and electrons) gives rise to new chemical pathways which ultimately results in a higher concentration of OH radicals, such as $O(^3P)+H_2O \rightarrow OH+ OH$, $O(^1D)+H_2O \rightarrow OH+ OH$ [38]. The sources of O (^3P) and O(^1D) are believed to be mainly from $O_2+e \rightarrow O(^3P)+ O(^1D)+e$ [39] , in which often involves the Herzberg and Schumann-Runge system of the O_2.

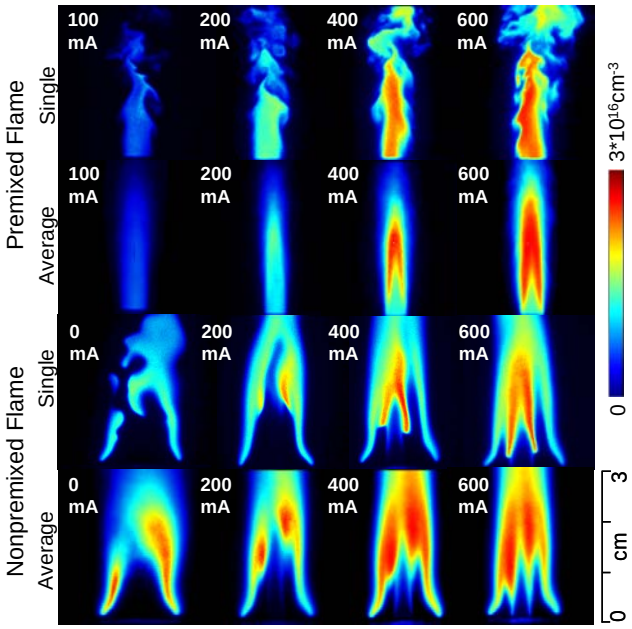

Figure 7. Single and averaged 2-D OH Planar Laser-Induced Fluorescence (PLIF) images as a function of increasing microwave power for both premixed flames (top) and non-premixed flames (bottom).

As can be in Figure 7, non-premixed flames show a unique two-cone flame structure: within the inner cone the main oxidation of the fuel with the air from the plasma discharge takes place; within the outer cone combustion with the ambient air also occurs. Overall, the height of the flame is larger for the non-premixed mode than for the premixed case while the flow appears to be more turbulent in the premixed flames due to the shorter reaction zone and subsequent non-premixed with the ambient air. As previously stated, the outer cone flame in the non-premixed mode can be sustained without any DC plasma power input for some of the lower flow rates used in this study. In the non-premixed flame, the reaction zone of the outer cone remains relatively constant as power is increased. However, the inner cone is dramatically increased as highly reactive air interacts with the fuel. At powers exceeding 400 mA, the OH

LIF intensity for inner flame front is much higher than the outer one, and the flame stability is dominated by the plasma discharge.

The influence of geometry and other parameters on the flame stability can also be observed from OH PLIF images. Figure 8 shows averaged OH PLIF images for both premixed and non-premixed flames at various flowrates and equivalence ratios. The top row shows a premixed flame with a rate of 12 SLPM, with equivalence ratios of ϕ= 0.7, 1.0 and 1.3. The bottom two rows shows a non-premixed mode flowrates of 6 SLPM (middle)/15 SLPM (bottom) with overall equivalence ratios of ϕ= 0.7, 1.0 and 1.3. In the premixed mode, the figures represented here are generally reproduced for all the flowrates where the flame is stable at the end of the plasmatron tip for leaner conditions; however, the flame tends to lift off at higher equivalence ratios (ϕ=1.3, top row in Figure 11). At high equivalence ratios, the radical pool is poorly established and fuel/air mixture tends to react more with ambient air resulting combustion downstream of the exit. Non-premixed flames at low (6 SLPM, middle row in Figure 8) do not reflect this phenomenon, and the flame is stable over a wide range of equivalence ratios. For higher total flowrates (15 SLPM bottom row in Figure 11), the stability of the non-premixed flame is compromised; the outer flame is no longer visible in the turbulent structure and the two flame zones merge into a single structure. The stability for these two configurations is different in that the premixed mode appears to be more chemistry driven and dependent on the equivalence ratio and the non-premixed mode is more dependent on the flowrates and the physical interaction of the fuel and the plasma discharge itself. Overall, the premixed mode can stabilize higher flowrates, but the smaller dimensions of the combustion and sensitivity on the fuel and air ratios can render the premixed mode more difficult to use for such plasma discharge systems.

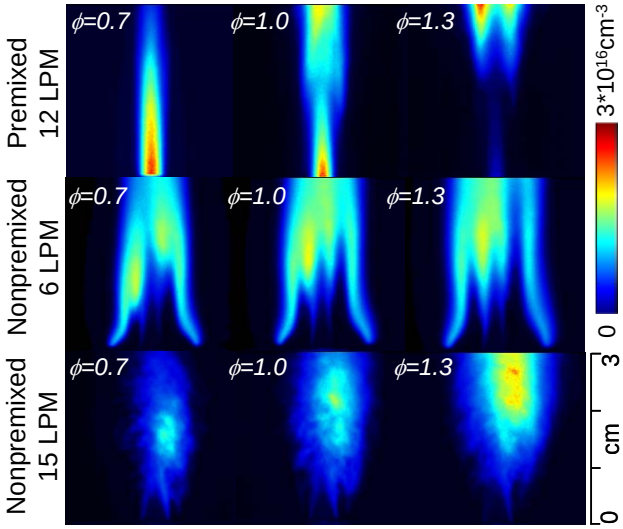

Figure 8. Averaged OH PLF images for all flowrates at premixed mode with ϕ= 0.7, 1.0 and 1.3 (top); Averaged OH PLF images for 6 LPM (middle)/15 LPM (bottom) at non-premixed mode with hi= 0.7, 1.0 and 1.3.

It is once again noted that this torch does not couple plasma energy efficiently into the reaction zone of the flame. The plasma is generated separately and the flame is ignited as the gases pass over the plasma region. The actual oxidation process occurs further downstream and outside of the torch. The following sections discuss an alternative concept of overlapping for focused electromagnetic field in the region of the flame itself. In section 5, this concept is further extended to investigate both premixed and non-premixed configurations for the direct coupling concept.

4 DEMONSTRATION OF DIRECT PLASMA COUPLING

In this study we investigate the novel concept of directly coupling electromagnetic energy into the reaction zone of an existing premixed flame for energetic enhancement of the combustion chemistry as show in Figure 9. The plasma generation process can be achieved with minimal power, as a high electric field is directly coupled to the electrons naturally present in a hydrocarbon-based flame. Once the plasma is generated, then it can mutually support the acceleration of flame chemistry and flame stabilization. Our goal is to understand the changes in the chemistry and temperature during this process including the impact of in-situ fuel reforming into CO and H_2, which is proposed as a key flame stabilization mechanism [40].

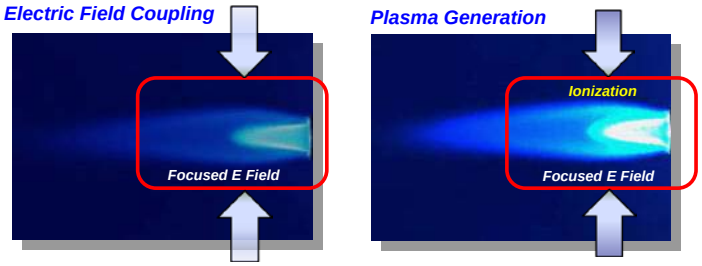

Figure 9. Schematic of direct plasma coupling (low mi crowave power (left), high microwave power (right)).

In order to demonstrate the direct coupling concept, an atmospheric high-Q re-entrant cavity applicator was designed and constructed to couple microwave (2.45 GHz) electromagnetic energy directly into the reaction zone of a premixed laminar methane-oxygen flame for flame enhancement [41-42]. Figure 10 shows the coaxial re-entrant cavity applicator: (a) displays a photograph of the system along with an inset picture of a methane/oxygen flame; (b) displays the corresponding schematic. The applicator is a brass re-entrant cavity excited with electromagnetic fields in the TEM quarter wavelength resonance mode. 2.45 GHz microwave energy is transmitted via a coaxial cable and emitted with a mono-pole antenna (Figure 10b). When the relative location of the torch, antenna, and baseplate are adjusted using the Unislide translators, an optimized resonant mode can be found wherein most of the energy is focused into the region between the edge of the outer cavity and the end of the combustion torch. Figures 10(c) show a numerical solution of Electric field using the program COMSOL MultiPhysics 3.4, which provides a relative 2-D electric field distribution within the coaxial cavity structure. The focus of the electromagnetic energy into the tip of the torch is enhanced as the radicals and the weak concentration of electrons in the flame amplify the coupling process. The unique features of this reactor are that it is able to sustain an atmospheric glow discharge in the reaction zone of the flame, but more importantly, the entire process is outside the cavity and in full view of laser and optical diagnostics.

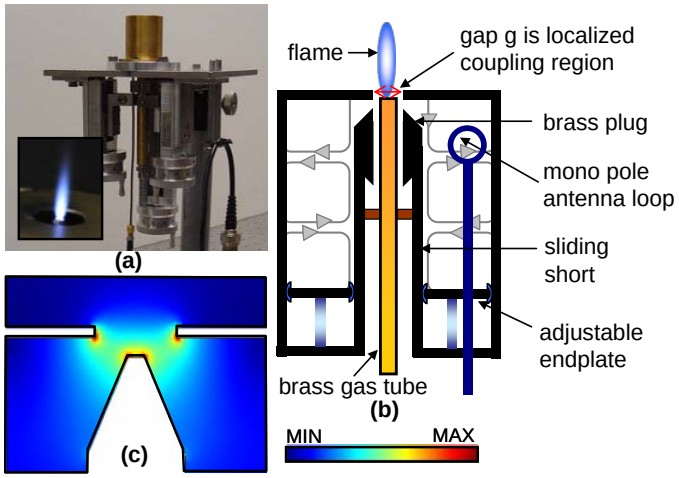

Figure 10. (a) Picture of coaxial re-entrant cavity applicator with picture of methane/oxygen flame shown in the inset; (b) Figure of the structure of the applicator; (c) Numerical simulation of electric field using COMSOL MultiPhysics

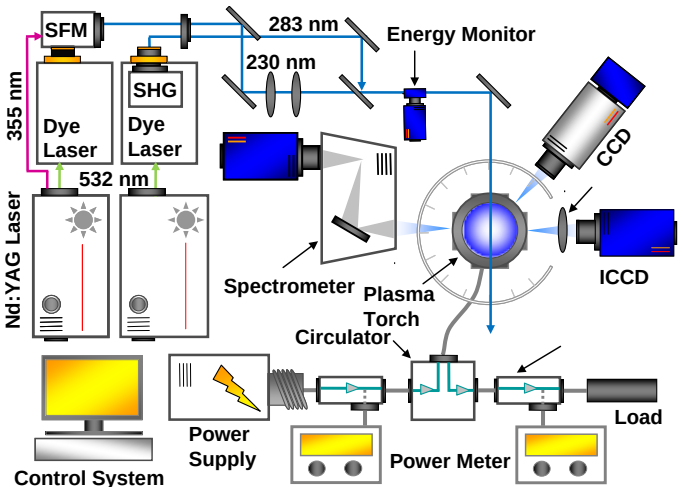

Figure 11. Experimental setup with bottom part shows microwave energy generation, coupling and monitor system.

Several optical diagnostic methods were used for temperature and species concentration measurements. A schematic of the experimental setup is shown in Figure 11. UV laser near 283 nm was used for planar laser-induced-fluorescence (PLIF) of OH using the $Q_1(8)$ transition from $A_2\Sigma^+ - X_2\Pi$ (1,0). The laser was expanded into a sheet and the fluorescence signal was collected at 90^o using an intensified CCD camera with a WG305 filter. The number density was derived by calibrating the signal to that of a Hencken Burner using a methane-air mixture. Here it was assumed that the fluorescence was in the linear regime; accordingly the OH number density was further corrected for differences in the rates for electronic quenching between the methane-oxygen flames and Hencken calibration flame using estimates of quenching rates from the OH A−X transition. CO in the reaction was measured using two-photon PLIF, pumping the $B_1\Sigma^+ - X_1\Sigma^+$ (0,0) transition at 230.10 nm. The fluorescence signal was imaged with an interference filter centered at 486nm with a bandwidth of 10nm. The number density is calibrated from a Chemkin simulation (mole fraction for 0W microwave power) using GRI-mech 3.0 with 1-D flame modeling with methane and oxygen. A McPherson 216.5 1-m spectrometer (entrance slit of 20 μm) was used for flame emission measurements and rotational OH thermometry. The emission was focused using a spherical lens (f=50 mm) through a pin-hole filter to isolate the reaction zone. A wide-range scan was conducted over a range of 250 to 550 nm at an increment of 0.5 nm to monitor the qualitative change in the population of excited state species.

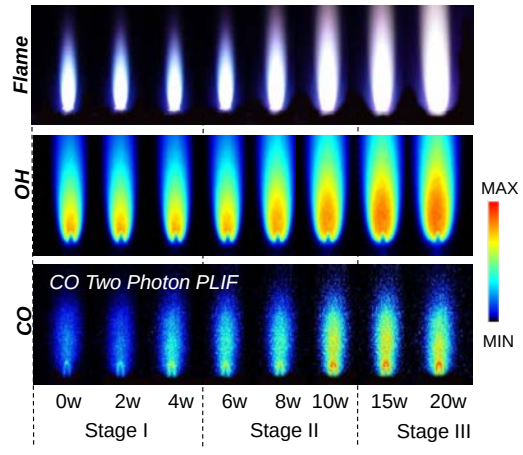

Figure 12. Photo (top), OH PLIF (middle) and CO PLIF (bottom) intensity images of CH4/O2 flame vs. microwave power with three stages noted (100 SCCM total flowrate at ϕ=1.1)

Photographs, 2-D OH PLIF and CO PLIF images of the flame are shown in Figure 12 as a function of increasing microwave power. At this condition, the fuel combustion power is 22 W using the lower heating value of methane. Overall, the flame luminosity and volume is increased as more microwave power is coupled into the flame region. At low powers the flame length is about 2 mm and a typical light blue hue is observed from the CH^* emission. As the power is raised to about 6 W, the microwave energy generates a distinctly different plasma plume with a purple emission that can be up to 10 mm in length (top row in Figure 12. From the OH images (middle row), it can be seen that the location of the reaction zone does not change dramatically, and a significant rise of OH in the post combustion gas region is evident. It is

expected that emission from the dramatic increased ionization and excited state species dominates the normal visible emission spectra at this point. In comparison, without the pilot flame for direct coupling, plasma plume generation would not occur at powers exceeding 100 W, and sustained flame stabilization would require more energy input. It can also be seen that the CO concentration rises through all three stages, indication that in-situ fuel reforming plays a key role in the ionization process (discussed in more detail below).

Number density of OH in the reaction zone of the flame is shown in Figure 13 as a function of microwave power (0 to 30 W). The progression of the plasma discharge as a function of microwave power can be divided into three distinct stages going from low power coupling to high. The stages also correspond to the one shown in Figure 12.

- *Stage 1:* "Electric Field Enhanced Stage": the OH does not show a noticeable increase. There is chemistry change here with fuel undergoing reformation and microwave energy coupling into the gas through vibrational excitation of nitrogen and elastic collisions. The electric field is expected to be around ~10^6 V/m at this stage and just below the threshold for breakdown of the hot gases.
- *Stage 2:* "Transition Stage": As the microwave field intensity increases, T_e exceeds T_g. High T_e and high reactivity lead to inelastic collisions for excitation, dissociation and ionization to generate new species and eventually to generate a plasma discharge. The plasma discharge from this stage is self sustained without a flame, and there is an explosive increase in the concentration of OH to about 5 times that of a typical premixed hydrocarbon flame.
- *Stage 3:* "Full Plasma Stage": At more than 10 W, the plasma volume grows larger and OH production remains relatively constant. At this stage, energy is coupled into other pathways as the formation of OH is saturated. The plasma discharge dominates the reaction one. Here, the termination and recombination reaction of the OH are balanced with the electron impact and ionization reactions initiated by the plasma discharge. Electron density in this state is expected to be on the order of ~10^{12} V/cm^3.

The addition of plasma has been shown to increase the flammability limit. From experiments we observed improvements in the flammability, although the flame enhancement is only through a weak electric field in Stage 1. At power levels of more than 6 W, the discharge could be sustained with only oxygen or methane and without combustion. As the ground state OH number density was not shown to increase in this stage, the improvement in the flammability limit is mainly assumed to be from temperature increase, which will be discussed further in the next section. Flame speed enhancement can be also shown by observing the change in the reaction zone contour as the flame velocity was changed. It was observed also that flame speed increases over all three stages.

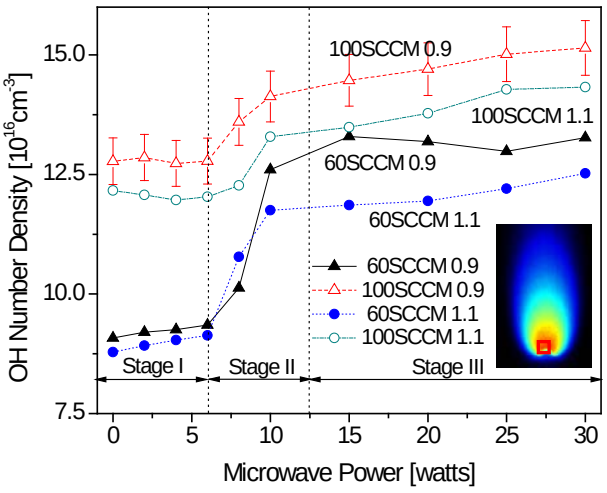

Figure 13. OH number density in burnt gas of CH_4/O_2 flame vs. microwave powers from averaged PLIF images

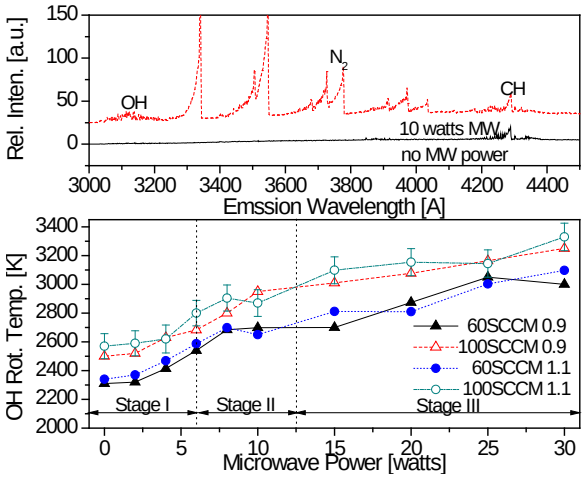

Figure 14. Emission spectra from CH4/O2 flame with no microwave radiation and 10 W microwave radiation (top) and OH rotational temperature at the same conditions as in Figure 14 (bottom).

In order to probe the changes in excited state species and temperature, spectrally resolved emission of the reaction zone was obtained. Figure 14 shows the emission spectra for the methane-oxygen flame with no microwave input and 10 W microwave input (top) and OH rotational temperature for different total flow rates and equivalence ratios (bottom). It is acknowledged that non-equilibrium degree in the plasma and chemical pumping routes may causes minor errors in the temperature evaluation.

In our measurements, it appears that a fraction (~5 to 10%) of indicated microwave energy was accounted for temperature increase (assuming constant specific heat and rotational temperature as kinetic temperature). The fraction for Stage 1 is higher than that for Stage 2 & 3. It is expected that kinetic effects play a larger role as the plasma is initiated, although even at Stage 1 changes in the chemistry of excited state metastables are observed.

In order to understand the impact of in-situ fuel reforming, we made measurements of CO concentrations using two-photon LIF, which are shown in Figure 15. The overall CO number density increases with microwave power for all conditions in Figure 15. In Stage 1, the in-situ fuel reforming (to hydrogen and carbon monoxide) as well as the temperature increase is expected to contribute to the enhancement in flammability limits and flame speed. CO production in rich flames is generally higher than that in lean flames. This is confirmed in the first data point (0W microwave power) of all four series. But in Stages 2 and 3 when microwave power is higher, CO number density at 100 SCCM with ϕ=0.9 is higher than that at 60 SCCM with ϕ=1.1 because at higher microwave power range, the effects of fuel breakdown from the plasma discharge surpass the thermal CO production in the flame.

It is important to quantify of the degree of fuel reforming assisted by the plasma. CO number density increases to 3.88 x 10^{17}cm^{-3} at the highest microwave power of 30 W, from 2.57 x 10^{17}cm^{-3} without microwave at the same flow condition (100 SCCM and ϕ=1.1). Mole fraction was calculated using rotational temperature in previous section, and CO mole fraction increases approximately to 15% from 9% without microwave in the same condition. Assuming that the water is in vapor state, in our configuration, 18% of the total methane undergoes reforming to syn-gas at 30W of microwave power, which is significant considering the competing oxidation reactions which subsequently leads to CO_2.

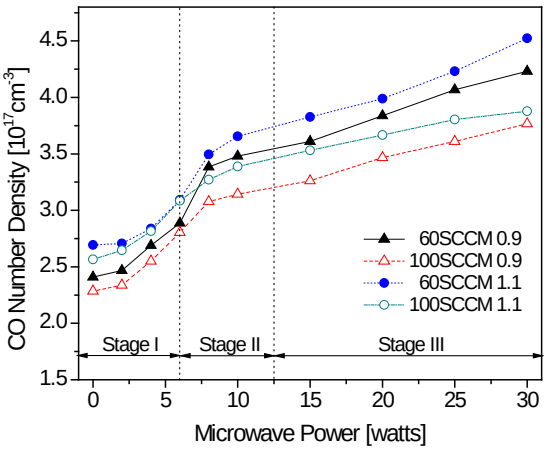

Figure 15. CO number density in burnt gas of CH_4/O_2 flame vs. microwave powers using CO Two-Photon Laser Induced Fluorescence

Re-ignition Process for Direct Plasma Coupled Flames

In this section, we investigate the conditions where the plasma discharge is self-sustained in the event that the pilot flame is extinguished using laser and optical diagnostics to identify the radical concentrations and thermodynamic state. Once the plasma is established it will act as the re-ignition source and the conditions of the plasma plume are once again characterized using optical measurements. The term re-ignition in here refers to ignition of premixed flow re-introduced to the plasma zone after the flame has been extinguished. The re-ignition phenomena which can occur in this highly efficient direct-coupled microwave plasma enhanced combustion system can provide a fundamental understanding of the relevant chemistry and thermodynamic influences and will contribute to the use of such concepts for practical systems in the future. The coaxial re-entrant cavity applicator used in this study is same as previously described in the preceding section [41-42] and only a brief description will be given here. The torch was developed for coupling microwave energy directly into the reaction zone as shown in Figure 12. The "direct plasma coupling" concept offers the advantage of efficient plasma initiation and stabilization at relatively low plasma power. Figure 11 shows a photo and schematic diagram of this microwave plasma applicator. The 2.45-GHz microwave energy is transmitted via a coaxial cable and emitted with a mono-pole antenna loop.

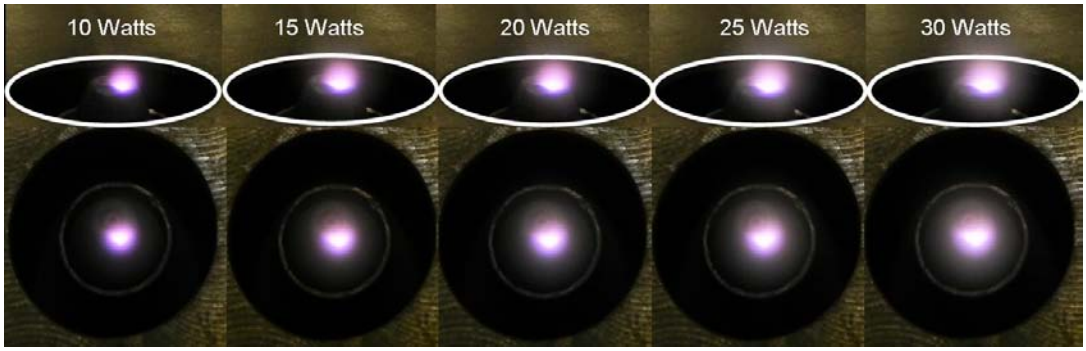

Figure 16. Images of the microwave air discharge vs. microwave power (top row taken from the side; bottom row taken from the top).

An atmospheric microwave ambient air plasma is initialed and stabled when gas flow is cut off the combustion system when microwave is larger than 10 W. Once the flame is extinguished and the plasma discharge is self-sustained in atmospheric air, it needs to act as the ignition source for the fuel and air mixture. A set of images of this discharge (without flame) at different microwave power levels is shown in Figure 16. The top row is taken from a side view and the bottom row is taken by looking straight down onto the torch. In the top row, a white circle is marked to show the edge of the cavity. A first observation is that the size and emission intensity increases with increased microwave power. Without the flame present, there is no dominant force to center the discharge and it wanders from side to side on the tip of the torch. In the air-discharge-only case shown in Figure 16, the electric field is high enough to sustain this air discharge even without the excess heat and radicals from a pilot flame. The electron density is estimated to be around $10^{12\text{-}13}$ cm^{-3} in these conditions [43].

Re-ignition phenomenon is observed when fuel/oxidizer is re-introduced into an atmospheric pressure plasma discharge generated by cutting off gas flow in a re-entrant microwave plasma applicator system. To investigate temporal evolution of flame initiation and stabilization during the re-ignition, a high speed camera was used. Figure 17 shows a series of

images for this re-ignition process at 20 Watts with a re-introduced reactant flow rate of 100 SCCM methane and oxygen with equivalence ratio of 1.1. The number on top of each image is the time, in miliseconds, starting at the onset of emission from oxidation reactions. The images were taken at repetitive rate of 10,000 Hz with exposure time of 50 μs. In a very short time after the first image, a faint 'ghost' flame quickly forms and then evolves to a smaller structure as the flame speed grows and the flame is stabilized. This effect is due to the initial breakdown of methane by the discharge: the microwave discharge is able to ignite the mixture but it has yet to fully couple with the plasma. After 25 ms, the plasma energy starts to couple into the flame which leads to a larger flame structure and reduction of the glow from the plasma discharge. The flame continues to grow in size and the total time for full stabilization in Figure 17 is about 900 ms.

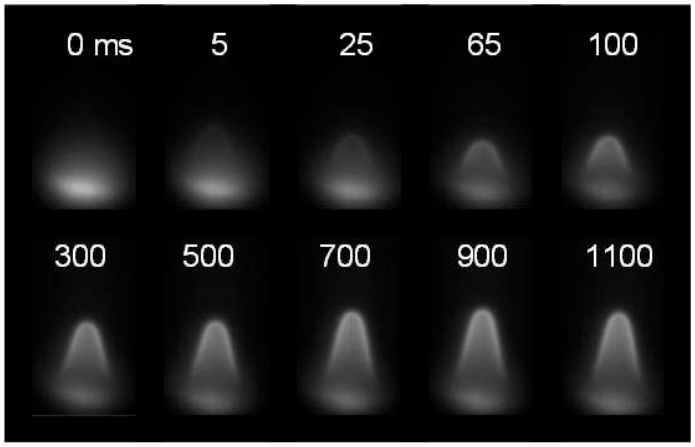

Figure 17. Set of images for re-ignition process at 20 Watts with a re-introduced total flow rate of 100 SCCM with equivalence ratio of 1.1.

5 DIRECT PLASMA COUPLED FLAMES IN A WAVEGUIDE BASED MICROWAVE PLASMA DISCHARGE

In the final year of the project, an effort was made to demonstrate the direct coupling of plasma energy into more realistic flame geometries and with higher combustion powers. The study addresses imaging of spatially resolved hydroxyl (OH) concentrations and temperature fields using planar laser-induced fluorescence and planar Rayleigh scattering, respectively. To achieve this, a new direct coupled plasma reactor was built and is shown in Figure 18.

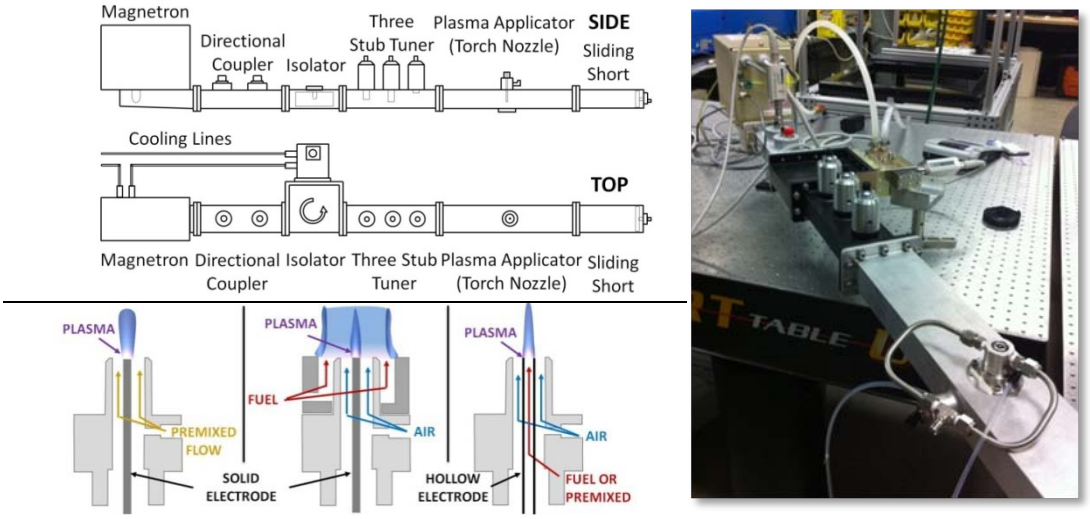

Figure 18. Microwave plasma reactor using a waveguide based co-axial structure. Left lower inset shows various configurations for both premixed and non-premixed plasma enhanced flames.

This new reactor extends the direct coupling concept to more realistic flow rates and flexible flame configurations. The plasma discharge system used in this study is based on a wave-guide coupled magnetron plasma torch and the combustor is designed for more than 2 kW of chemical energy conversion. The method of E-field generation in this reactor is based on a waveguide to channel the microwaves (in the fundamental mode) from a magnetron head after which the power is delivered to the tip of the torch through a co-axial antenna. The plasma is generated at the tip of the torch and fully accessible to optical measurements (T_g < 1200 K in air plasma, n_e~10^{14}-10^{15} cm^{-3}). The power supply is a 2 kW magnetron (2.45 GHz), although no more than 40 W seems to be required for most test conditions due to the high coupling efficiency. The reactor tube itself acts as the outer electrode, and the microwave power is delivered to the top surface by adjusting the standing waves using a sliding short at one end and a 3-stub tuner on the other. The directional coupler monitors the reflected power from the reactor. The new reactor can accommodate a range of different flames (both premixed and non-premixed) and electrode configurations as shown in the lower left section of Figure 18.

Laser & Optical Diagnostics

In order to understand the interaction of the plasma discharge and the flame chemistry, laser and optical measurements involving radical concentration (OH) measurements and temperature imaging were applied. OH was excited using the $Q_1(8)$ transition of the $A^2\Sigma^+ - X^2\Pi$ (1,0) band, which requires narrowband UV light near 283 nm [44]. The measurements were conducted

using a dye laser (Lumonics Hyperdye HD-300) with an output of 7 ns pulses at 566 nm, which was subsequently frequency doubled through an Inrad Autotracker (ATIII) to frequency the desired excitation wavelength of 283 nm. The laser is pulsed at 10 Hz and has a spectral line width of about 0.1 cm^{-1} at 283 nm. The pulse energy was recorded digitally using a fast photodiode and an oscilloscope and attenuated (using a combination of a polarizing beam splitting and a half-wave plate) to ensure operation within the linear fluorescence regime. The laser was expanded into a sheet, and the fluorescence signal was collected at 90° using an intensified CCD camera (Roper Scientific Superblue PIMAX) fitted with a Cerco 45-mm focal-length, f/1.8 lens and a high-transmission (>80% at 310 nm) bandpass filter (Custom fabrication – Laser Components GmbH). A PMT coupled to a small spectrometer with collection optics focused on a flat flame burner was used to identify excitation spectra and monitor the laser wavelength. A Hencken burner was used to correlate the signal intensity with the OH number density using previously performed absorption measurements.

Rayleigh scattering thermometry was conducted using the frequency doubled output of an Nd:YAG laser (λ=532 nm). Scattering measurements were used here, rather than other thermometry methods that are based on assumptions of the population of quantum states, due to the non-equilibrium nature of the plasma discharge. Scattering was collected through a bandpass filter centered at 532 nm with a 10 nm FWHM using a second intensified CCD camera (Roper Scientific Gen III PIMAX) fitted with a Nikon 58-mm focal length f/1.2 Noct-Nikkor lens. Black curtains enclosed the test section to limit background scattering, and sufficient signal quality was achieved so that Filtered Rayleigh scattering approaches were not required. The collected scattering is a measure of number density from which a planar temperature profile can be obtained utilizing the Ideal Gas Law. By normalizing the images by an image of Rayleigh scattering in air with no discharge, the laser intensity is eliminated from the calculation. The temperature is given by

$$T_d = \frac{\sigma_d I_a}{\sigma_a I_d} T_a \tag{1}$$

where σ_d and σ_a are the respective Rayleigh scattering cross sections of the discharge gas and air. I_a is the reference scattering intensity in air at temperature T_a, and I_d is the scattering intensity from the plasma discharge. For combustion cases, gas composition in the reaction zones was assumed to be the stoichiometric products of methane/air, which limits error due to composition assumptions to less than 10%, as nitrogen is still the primary constituent. For air plasmas, composition of dry air was used for the cross sections. To reduce Mie scattering (as particles could not be eliminated due to mixing with the room air), the camera was positioned to collect backscattering, and averaged images were calculated as the median of 200 images (based on the median signal value of each pixel).

The MW power level is defined as the difference between measured incident and reflected power. A desired power level was achieved by adjusting the tuning components to achieve a reflected power corresponding to the desired absorbed power level. The incident power remained fixed at about 360 W, the lowest possible value for the power source. Losses were assumed to be minimal and not accounted for, as the power level values are used for relative comparison and not absolute calculations in the study. We have verified through temperature measurements in the waveguide that most of the energy is deposited into the torch and no perceivable heating of the waveguide system is detected.

Solid Electrode and Premixed Flame

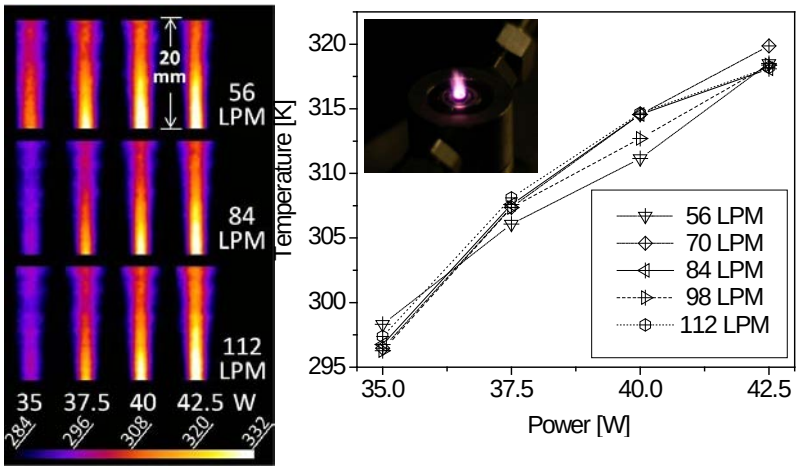

Figure 19. Images of average temperature [K] of an argon plasma discharge for varying microwave power levels and flow rates (left), plot of temperature [K] versus power [W] for multiple flow rate.

It is important to verify that the current reactor configuration of delivering microwave energy for plasma generation is capable of generating a 'cold-plasma' with a high degree of thermal non-equilibrium. For demonstration, a non-equilibrium plasma was produced using the solid electrode configuration with pure argon flowing through the nozzle. The discharge was initiated at absorbed power levels of 35 W and flow rates of 56 to 112 LPM (60 to 125 m/s), much lower power levels and higher flow rates than plasmas of air and fuel. A cold argon plasma can be sustained, at temperatures near ambient conditions. After the plasma is initiated, increases in power level quickly produce a temperature increase in and around the plasma. Figure 19 graphically illustrates and plots the discharge temperate for various power levels and flow rates. Plotted data are the mean values of a small (1 mm × 0.75 mm) maximum temperature region extracted from the median image for a given condition. The ability to a generate low power, low temperature plasma at atmospheric pressure has been of interest as a sterilization method, particularly for heat sensitive materials for which traditional sterilization is not suitable [45-46]. The non-thermal nature of the argon plasma contrasts sharply with measurements of an air-only plasma. When the torch is operated with a flow composition of solely air, temperatures were measured in excess of 3000 K. Additionally, inclusion of small amounts of oxygen or methane into the argon flow immediately raised the plasma temperature.

A premixed flame was ignited and sustained by a microwave plasma discharge using the solid electrode configuration. Microwave power, flame equivalence ratio, and total flow rate were individually varied as data was collected. A microwave discharge could be observed at an absorbed power of about 70 W, igniting and sustaining a flame for all tested flow rates, from 5 to 20 LPM (5.5 to 22.1 m/s). After ignition, the plasma discharge is stable down to power levels of 60 W. The flame is not stable without the plasma discharge, and blow-off is observed if the plasma is extinguished by detuning the waveguide.

For OH concentration calculations, the Boltzmann

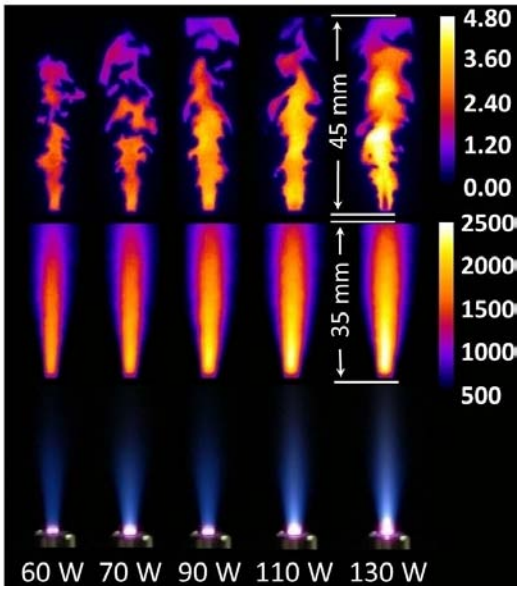

Figure 20. Images of OH number density [10^{16} cm^{-3}] (top), averaged temperature [K] (middle), and photographs of discharge (bottom), of a solid electrode premixed discharge for varying microwave power levels, increasing left to right (15 LPM total flow rate).

fraction was considered constant, an adequate assumption for temperatures in the range of 1050 K to 2600 K, as the population varies less than 10% from the calibration flame value. Additional error is expected outside of this range, where an under-prediction of OH occurs due to lower state populations. Figure 20 displays a series of OH concentration and temperature images with power increasing from 60 to 130 W. There is a clear increase in OH number density and T as the cavity is tuned to increase the absorbed power. Average temperature increased from approximately 2150 to 2650 K as power was increased from 60 to 130 W. Maximum hydroxyl concentration increased from 3 to 4.6 $\times 10^{16}$ cm^{-3} for the same power interval. The increase in excited state species produced by plasma chemistry expands the chemical pathways to OH production. For example, oxygen in the form of $O(^3P)$ and $O(^1D)$ is produced via $O_2+e \rightarrow O(^3P)+O(^1D)+e$ [39] and contributes to OH radical concentration through reaction with water vapor $O(^3P)+H_2O \rightarrow OH+OH$, $O(^1D)+H_2O \rightarrow OH+OH$ [38].

Solid Electrode and Non-Premixed Flame

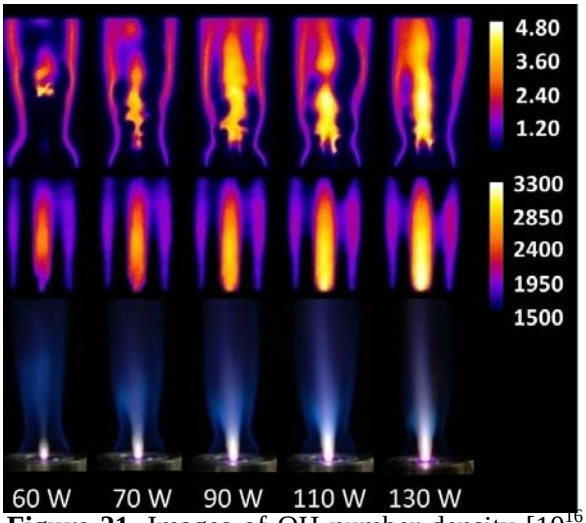

Figure 21. Images of OH number density [10^{16} cm^{-3}] (top), averaged temperature [K] (middle), and photographs of discharge (bottom), of a solid electrode non-premixed discharge for varying microwave power levels, increasing left to right (1 LPM fuel, 5 LPM air flow rate).

A non-premixed flame was produced with the addition of a coflow adaptor. Air flow through the nozzle was a constant 5 LPM yielding a speed of 5.5 m/s. Fuel flow through the coflow adaptor (annular surrounding the nozzle) varied from 0.5 to 2.0 LPM (0.4 to 1.4 m/s). Air is injected in the center of the nozzle while a jet of fuel is injected around the circumference. There are two flame fronts in this configuration. The inner front is caused by fuel entrainment into an air plasma plume whereas the outer front is a typical flame with the surrounding air. The OH number density along the inner front increases with power and is similar in magnitude to the solid electrode premixed case. The OH density in the outer front is much lower, in the expected range for a diffusion flame. OH number density, temperature, and photographs of a non-premixed, plasma assisted combustion configuration can be seen in Figure 21.

The maximum OH concentration is located within the inner flame front and is largely a function of power, ranging from (2−5) $\times 10^{16}$ cm^{-3} for power levels of 60 to 110 W. This is the same range of OH concentration measured previously in a solid electrode premixed configuration. The inner flame height is reduced as power is increased, transitioning from a lifted flame to stable flame at the plasma plume tip as the flame speed increases. The maximum temperature is in excess of 3500 K at 130 W. Plasma energy has mostly a thermal effect on the airstream, heating it to a greater degree than the methane-air premixed flame. The spatial location of the outer and inner reaction fronts are marked clearly by maxima in both OH number density and temperature as seen in Figure 22. Asymmetries are due to the imperfections in coflow adaptor symmetry, and thus, asymmetries in the flow. Furthermore, the camera used for Rayleigh scattering was positioned at a different angle than that used for OH PLIF, resulting in different asymmetries observed in the studies. Temperature images were corrected for the non-perpendicular camera placement using an image of a target grid.

The plots confirm the general trends noted in the premixed case; Increases in power lead to increases in OH density and temperature. Without microwave power, a flame can be stabilized only if there is no nozzle flow. The increase in OH density is both a function of increasing temperature and flame front movement toward the torch. The temperature is observed to be sufficiently high for combustion at this power; regardless, it can be seen that OH propagation is not very high at even these temperature due to the insufficient mixing.

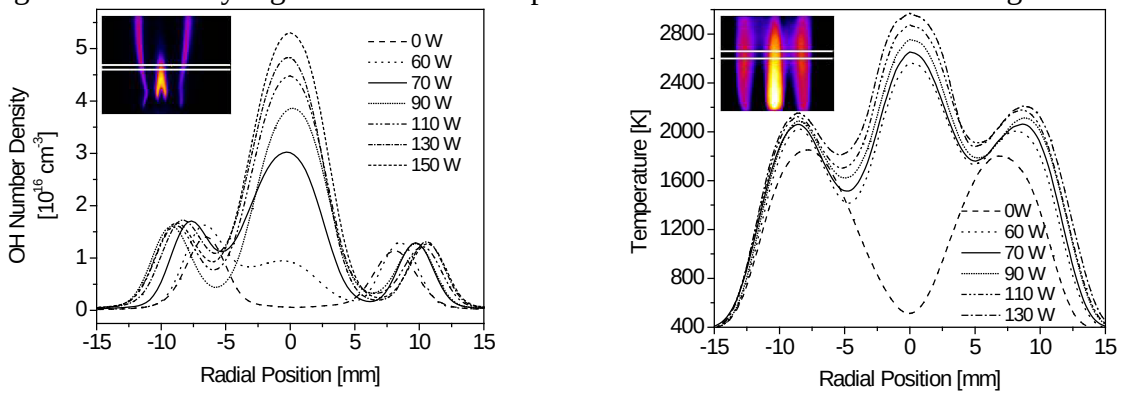

Figure 22. OH number density (left) and temperature (right) profiles of the solid electrode non-premixed plasma discharge for varying power levels. Inset images depict data extraction area (25 mm over torch).

Hollow Electrode and Non-Premixed

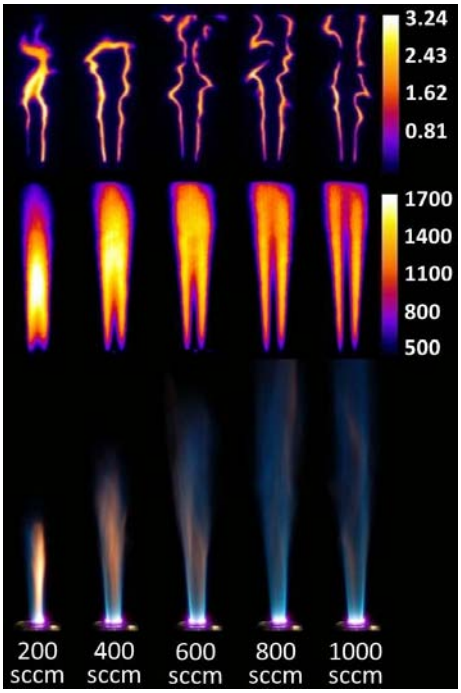

Figure 23. Images of OH number density [10^{16} cm^{-3}] (top), averaged temperature [K] (middle), and photographs of discharge (bottom), of a non-premixed discharge for varying hollow electrode fuel flow rates, increasing left to right (70 W).

Methane was sent through the hollow electrode while air passed through the nozzle around the electrode. The plasma discharge formed on the boundary between the two flows, igniting a non-premixed flame where fuel and air mix. The motivation for a hollow nozzle is mainly due to the fact that the highest concentration of E-field is at the tip of the electrode and a hollow nozzle would direct most of the gas directly into the plasma plume. OH number density and temperature were recorded for different microwave powers and fuel flow rates from 200 to 1000 sccm (1.4 to 6.9 m/s). Nozzle air flow around the electrode was fixed at 30 LPM (12.2 m/s). Figure 23 contains a graphical representation of the data for a power level of 70 W.

OH number density images clearly show a flame front along the methane-air interface, as expected for a non-premixed flame. As fuel flow rate increases, the front stretches, and extends out of the field of view by 600 sccm. The images show apparent local flame extinction and greater front curvature at increasing fuel flow rate. Average OH images (not shown) look very similar to the temperature images from the Figure 23. Maximum OH radical concentrations range from (1.5-4.5) $\times 10^{16}$ cm^{-3} as power is increased from 70 to 130 W but show little dependence on flow rate. For this configuration, the highest median temperatures are not located at the plasma,

but downstream, where additional heat from oxidation is released. Increasing the microwave power level has no effect on the median temperature values.

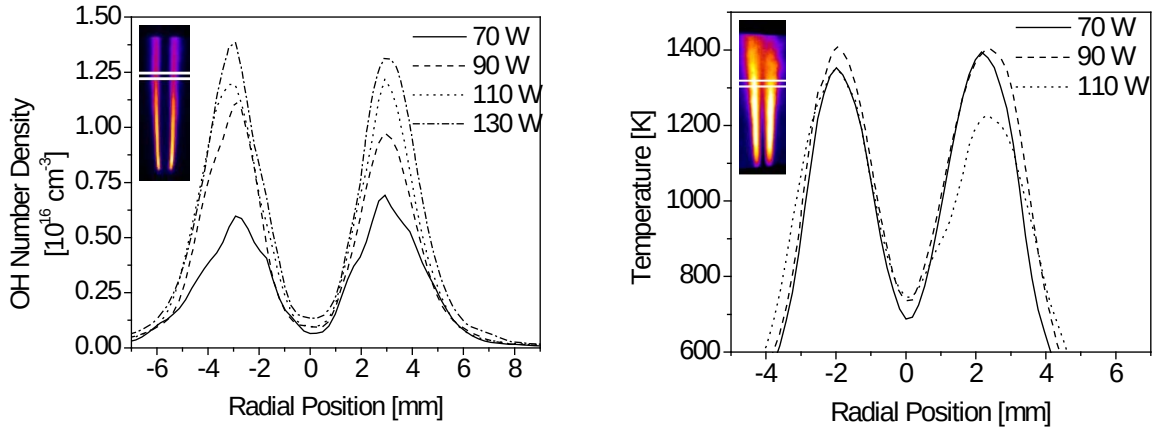

Figure 24. OH number density (left) and temperature (right) profiles of the non-premixed hollow electrode plasma discharge for varying power levels. Inset images depict area of data extraction (25 mm above the torch tip, 600 sccm fuel flow rate).

OH number density and temperature profiles at 25 mm above the torch tip are plotted in Figure 24. There are two maxima for each line indicating the location of the cylindrical flame front. OH radical concentrations increase significantly at each power level while median temperature remains nearly constant. This indicates that adding microwave energy to this plasma coupled flame can increase OH radical concentration without significant thermal effects, in contrast to observations of solid electrode configurations. The large increase in OH concentration is likely due to incomplete combustion at low powers, as evident by the observation of soot. The relatively constant temperature is unique to hollow electrode configuration and contrasts sharply with what was observed in the solid electrode non-premixed case, where the plasma was surrounded by airflow while the fuel flow surrounded the nozzle annularly. These results, along with previous comparisons of air only plasma and a CH_4-air plasma coupled flame, suggest gas flow heating is greater in configurations where the plasma is formed in air than at the methane-air interface.

Hollow Electrode and Premixed

A second hollow electrode flame was studied by flowing a premixed methane-air gas through the electrode. The total premixed flow rate was held constant at 2 LPM (13.8 m/s) while the microwave power and equivalence ratio varied. Figure 25 contains images of OH number density and temperature for a hollow electrode premixed flame at a power level of 100 W for different fuel-rich equivalence ratios. The photographs show the flames have a long conical structure that lengthens as the equivalence ratio increases. The OH profiles show a cylindrical flame front, thicker than that observed in the non-premixed case, with a maximum concentration range of (1.0-4.0) $\times 10^{16}$ cm^{-3}. OH number density is inversely related to equivalence ratio, with maximum concentrations 10 to 20 % greater for flames with an equivalence ratio of 2.0 than 8.0. Median temperature images also show a decrease in temperature as fuel fraction increases, ultimately approaching temperatures seen in the non-premixed flame as the fuel fraction becomes very large. The hollow electrode with premixed

flow allows for reliable ignition and stable combustion of a very rich flow without sooting at velocities greater than 10 m/s.

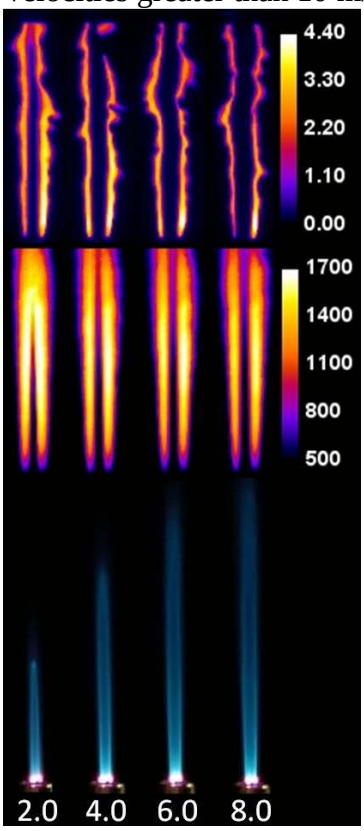

Figure 25. Images of OH number density [10^{16} cm^{-3}] (top), averaged temperature [K] (middle), and photographs of discharge (bottom), of a premixed discharge for varying hollow electrode flow equivalence ratio (100 W).

Figure 26 contains plots of OH concentration and temperature 25 mm above the torch tip. Peak OH number density scales nearly proportional to microwave power. A 50 % increase in power, from 80 W to 120 W, yields a 60 % increase in peak OH number, whereas temperature increases by about 15 %. Also plotted are temperature profiles for 3 downstream locations for a premixed flame with a equivalence ratio of 6.0 and 90 W of microwave power. It is observed that the median temperature increases moving away from the torch. The plasma ignites the flow, but most of the heat release occurs downstream as the fuel continues to oxidize.

Temperature profiles suggest plasma induced initial fuel cracking and continued oxidation downstream. This configuration offers the greatest advantage of targeted energy deposition into a fuel rich flow to initiate combustion through CH_4 decomposition. Studies of the kinetic mechanisms of plasma-based CH_4 conversion have produced data outlining in-situ fuel reformation pathways of interest for plasma assisted combustion [47-48]. A non-equilibrium plasma facilitates additional pathways for CH_4 decomposition, including CH_4 excitation via electron impact and subsequent breakup. Energetic nitrogen species actively initiate oxidation: $CH_4+N_2(A, \nu=1)$ or $CH_4+N_2(X, \nu>20)\rightarrow CH_3+H+N2$. Active in OH radical production and a product of oxygen disassociation by electron impact, $O(^1D)$ also reacts with CH_4 at low temperatures: $CH_4+O(^1D)\rightarrow CH_3+OH$.

In our studies, this configuration resulted in the most stable flame stabilization at high velocities in excess of 10 m/s. The main reason for this is attributed to flow of the fresh gases directly into the focused zone of the e-field, and also that rich mixtures can result in fuel reforming effects which directly lead to enhanced combustion chemistry. Actual implementation of such a system a propulsion system should take into consideration of a similar design.

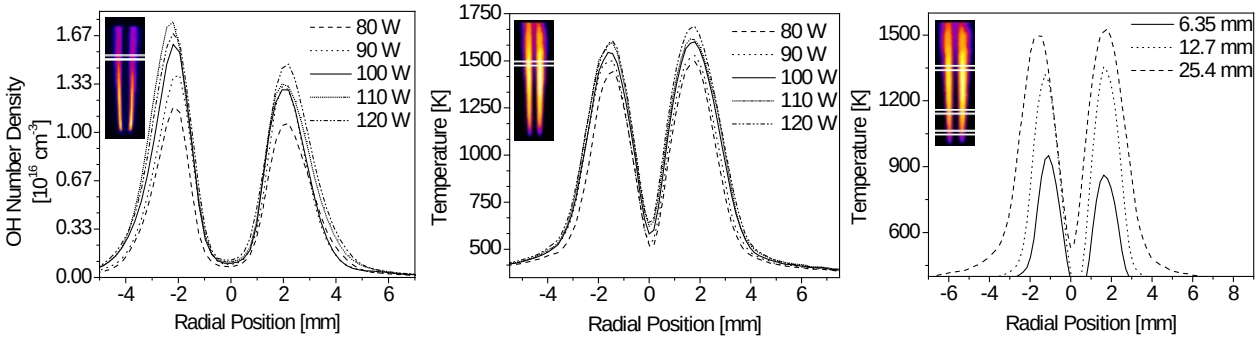

Figure 26. OH number density (left) and temperature (center) profiles of the premixed hollow electrode plasma discharge for varying power levels with inset images depicting area of data extraction (25 mm over torch). Temperature profile at three downstream locations in a flame with an equivalence ratio of 6.0

and microwave power level of 90 W (right).

6 CONCLUSION

This study was aimed at applying advanced laser imaging and optical diagnostics to study the physicochemical impact of nonequilibrium plasmas to enhance the conversion of chemical energy in combustion, and to investigate new efficient concepts for coupling plasma energy into a flame, seeking future potential application in high speed engines including scramjets. The main research achievement of this study was in investigating a new direct coupling strategy of focusing the energy right into the reaction zone of the flame.

To demonstrate this concept, an atmospheric high-Q re-entrant cavity applicator was designed and constructed to couple microwave (2.45GHz) electromagnetic energy directly into the reaction zone of a premixed laminar methane-oxygen flame for flame enhancement, where ionization of the reaction zone is achieved with power levels as low as 6 W. PLIF imaging of OH and CO are conducted in the reaction zone over this transition, as well as spectrally resolved flame emission measurements to monitor excited state species and determine temperature conditions. Re-ignition conditions for the plasma discharge are also examined. The efforts were extended to more realistic flame geometries in a new waveguide based microwave plasma reactor where both premixed and non-premixed flames could be energetically enhanced using a non-equilibrium discharge. OH number densities and temperature fields were measured using PLIF and Rayleigh scattering, respectively. In all conditions, increases in OH radical density and temperature as functions of power are observed. Premixed flames where a fuel rich mixture injected directly into the plasma region showed significant improvement in flame stability where effects of non-thermal kinetic and fuel reforming effects were dominant.

Additionally, this study investigated nitric oxide generation in a transient arc DC plasmatron using laser and optical diagnostics. Measurements of NO were made over a wide range of flow conditions and input plasma power levels. The concentrations in the imaging field were quantified using a multi-line calibration method involving spectroscopic modeling of NO LIF. Results show that NO formation in the igniter with high to moderate plasma energy coupling in a flame is considerable higher than that predicted by normal thermal mechanisms, but still an order of magnitude lower than cases where a plasma discharge is present without a flame. In addition to the NO imaging, flame dynamics for premixed and non-premixed configurations in the DC plasmatron were also investigated.

7 FUTURE PLANS

Future diagnostics plans for the plasma enhanced reactor are outlined in Figure 27.

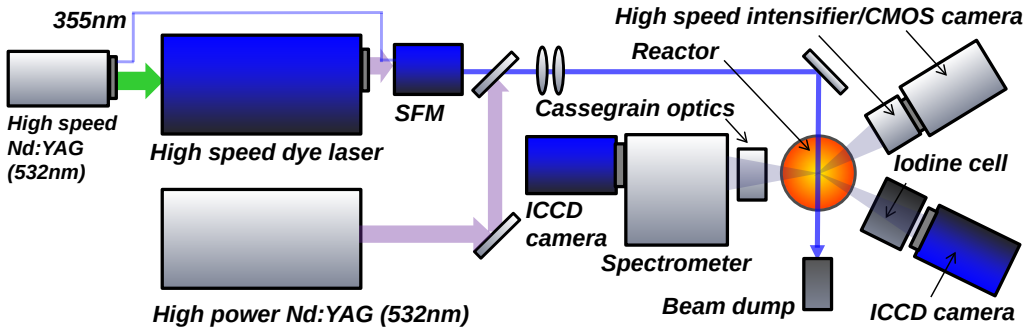

Figure 27. Schematic of the experimental setup including direct coupled MW plasma reactor and laser based diagnostics equipment.

The following measurements will be conducted to further enhance our understanding of the plasma-flame interaction and to support advanced numerical simulations outline below.

- ***Chemical Species Imaging***: High speed imaging of radicals at ***kHz rates*** to resolve evolution and propagation of chemical species during enhanced chemical energy conversion
- ***Temperature Field Imaging***: Imaging of temperatures both inside and beyond the reaction zone for a wide range of flow rates and electromagnetic energy levels.
- ***E-field and Plasma Characterization***: Imaging of excited state species, degree of non-equilibrium, and characterization of the electron density in the reaction zone. A Cassegrain optical system will be used to deduce plasma parameters from specific locations in the reaction zone.

Support of Numerical Simulation Efforts: The experimental efforts outlined here will be used to support simulation efforts within the US Air Force Research Laboratory (Kirtland AFB) using the Improved Concurrent Electromagnetic Particle-In-Cell (ICEPIC) code [49-53]. ICEPIC is a fully kinetic electromagnetic massively parallel Particle-In-Cell (PIC) code, which has an associated Monte Carlo (MC) package for modeling collisional interactions. The MC package is capable of handling both neutral and charged particle collisions, as well as the full range of interactions between various species. Using ICEPIC, the goal is to achieve sufficient understanding of the reaction routes of the energetic electrons, which we can use to optimize the system to maximize energetic enhancement of the combustion chemistry. Also, the detailed spatial data from our PLIF imaging, as well as temperature and electric field strength measurements will provide a benchmark for validating the multi-D capability of ICEPIC. The efforts will be carried out in joint collaboration with Dr. Andrew Christlieb who is an IPA with AFRL Kirtland and has access to AFRL systems for running large-scale 2-D cylindrically symmetric ICEPIC simulations of microwave driven CH_4/air plasmas at atmospheric pressure.

8 ACKNOWLEDGEMENTS

Much of the work discussed here was carried out in collaboration with the Propulsion Directorate at Wright Patterson Air Force Base. Dr. Lee has spent 8 weeks at the Aerospace Propulsion Division of the Propulsion Directorate in 2009, 2010, and 2011 working with Dr. Campbell Carter (also with Dr. Jim Gord and Dr. Sukesh Roy in 2010 and 2011) on much of laser diagnostics measurements discussed here. We are grateful for the support from AFRL and scientific guidance which has resulted in this work.

9 PERSONNEL SUPPORTED

Faculty

Professor Tonghun Lee

Graduate Students

Stephen Hammack (Ph.D. student)

Xing Rao (Ph.D. student, graduated in December of 2010)

Zachery Williams (M.S. student, graduated in May of 2011)

10 PUBLICATIONS FROM THIS GRANT

1. S. Hammack, C. Carter, T. Lee, *Direct Coupled Plasma Assisted Combustion using a Microwave Waveguide Torch*, IEEE Transactions, Special Issue on Plasma Science, accepted and in print (2011).
2. X. Rao, S. Hammack, T. Grotjohn, J. Asmussen, C. Carter, T. Lee, *Microwave Plasma Coupled Re-Ignition of Methane and Oxygen Mixture under Auto-Ignition Temperature*, IEEE Transactions, Special Issue on Plasma Science, accepted and in print (2011).
3. X. Rao, S. Hammack, C. Carter, T. Lee, *Laser Diagnostics of Energetically Enhanced Flames using Direct Microwave Plasma Coupling*, IEEE Transactions on Plasma Science, 39, 11, 2354-2355 (2011).
4. X. Rao, S. Hammack, C. Carter, I. Matveev, T. Lee, *Flame Dynamics of Plasma Enhanced Premixed and Non-Premixed Flames*, IEEE Transactions, Special Issue on Plasma Science, 38, 12, 3265-3271, (2010).
5. X. Rao, K. Hemawan, C. Carter, I. Wichman, T. Grotjohn, J. Asmussen, T. Lee, *Combustion Dynamics for Energetically Enhanced Flames using Microwave Energy Coupling*, Proc. Comb. Symp. 33, 2, 3233-3240 (2010).
6. X. Rao, I. Matveev, T. Lee, *Nitric Oxide Formation in a Premixed Flame with High Level Plasma Energy Coupling*, IEEE Transactions, Special Issue on Plasma Science, 37, 12, 2303-2313 (2009).
7. S. Hammack, X. Rao, C. Carter, Z. Williamson, T. Lee, *Laser Diagnostics of Plasma Enhanced Flames in a Waveguide Microwave Discharge System*, 49th Aerospace Sciences Meeting, Orlando FL, Jan., AIAA-2011-1019 (2011).
8. X. Rao, K. Hemawan, C. Carter, T. Grotjohn, J. Asmussen, T. Lee, *Plasma Enhanced Combustion using Microwave Energy Couping in a Re-entrant Cavity Applicator*, paper AIAA-2010-0651 at 48th Aerospace Sciences Meeting, Orlando FL, Jan. (2010).
9. X. Rao, I. Matveev, T. Lee, *Nitric Oxide Fomation during Ignition and Combustion of a Transient Arc Plasmatron*, paper AIAA-2009-0228 at 47th Aerospace Sciences Meeting, Orlando FL, Jan. (2009).

11 REFERENCES

1. W. H. Heiser, and D. T. Pratt, Hypersonic Airbreathing Propulsion, (AIAA Education Series, 1994).
2. E. T. Curran, and S. N. B. Murthy, Scramjet Propulsion, (AIAA, Progress in Astronautics and Aeronautics, 2000).
3. J. Li, F. Ma, V. Yang, K. C. Lin, and T. A. Jackson, "A Comprehensive Study of Combustion Oscillations in a Hydrocarbon-Fueled Scramjet Engine," 45th AIAA Aerospace Sciences Meeting and Exhibit**,** AIAA 2077-2836 (2007).
4. A. Ben-Yakar, and R. K. Hanson, "Cavity flame-holders for ignition and flame stabilization in scramjets-An overview," Journal of Propulsion and Power **17,** 869-877 (2001).
5. S. B. Leonov, and D. A. Yarantsev, "Plasma-induced ignition and plasma-assisted combustion in high-speed flow," Plasma Sources Science and Technology **16,** 132-138 (2007).
6. S. M. Starikovskaia, "Plasma assisted ignition and combustion," Journal of Physics D: Applied Physics **39,** R265-R299 (2006).
7. K. W. Hemawan, C. L. Romel, S. Zuo, I. S. Wichman, T. A. Grotjohn, and J. Asmussen, "Microwave plasma-assisted premixed flame combustion," Appl. Phys. Lett. **89,** 141501 (2006).
8. J. Liu, F. Wang, G. Li, A. Kuthi, E. J. Gutmark, P. D. Ronney, and M. A. Gundersen, "Transient Plasma Ignition," IEEE Trans. on Plasma Science **33,** 326-327 (2005).
9. F. Wang, J. B. Liu, J. Sinibaldi, C. Brophy, A. Kuthi, C. Jiang, P. Ronney, and M. A. Gundersen, "Transient Plasma Ignition of Quiescent and Flowing Air/fuel Mixtures," IEEE Trans. on Plasma Science **33,** 844-849 (2005).
10. A. B. Leonov, D. A. Yarantsev, A. P. Napartovich, and I. V. Kochetov, "Plasma-assisted ignition and flameholding in high-speed flow," in *44th AIAA Aerospace Sciences Meeting, AIAA-2006-563*, AIAA-2006-563 (Reno, Nevada, 2006).
11. L. Bromberg, D. R. Cohn, A. Robinovich, and N. Alexeev, "Plasma Catalytic Reforming of Methane," Inter. J. of Hydrogen Energy **24,** 1131-1137 (1999).
12. C. S. Kalra, A. Gutsol, and A. Fridman, "Gliding arc discharge as a source of intermediate plasma for methane partial oxidation," IEEE Transactions on Plasma Science **33,** 32-41 (2005).
13. G. Lou, A. Bao, M. Nishihara, S. Keshav, Y. G. Utkin, J. W. Rich, W. R. Lempert, and I. V. Adamovich, "Ignition of Premixed Hydrocarbon-Air Flows by Repetitively Pulsed, Nanosecond Pulse Duration Plasma," Proc. Comb. Inst. **31,** 3327-3334 (2007).
14. F. J. Weinberg, K. Hom, A. K. Oppenheim, and K. Teichman, "Ignition by plasma jet," Nature **272,** 341-343 (1978).
15. W. Kim, H. Do, M. G. Mungal, and M. A. Capelli, "Flame stabilization enhancement and NOx production using ultra short repetitively pulsed plasma discharge," in *44th AIAA Aerospace Sciences Meeting and Exhibit, AIAA-2006-560* (2006).
16. T. Ombrello, X. Qin, Y. Ju, A. Gutsol, A. Fridman, and C. Carter, "Combustion Enhancement via Stabilized Piecewise Nonequilibrium Gliding Arc Plasma Discharge," AIAA J. **44,** 142-150 (2006).
17. W. Kim, H. Do, M. G. Mungal, and M. A. Cappelli, "Plasma-Discharge Stabilization of Jet Diffusion Flames," IEEE Transactions on Plasma Science **34,** 2545-2551 (2006).
18. N. Chintala, A. Bao, G. Lou, and I. V. Adamovich, "Measurements of combustion efficiency in nonequilibrium RF plasma-ignited flows," Combustion and Flame **144,** 744-756 (2006).

19. W. Kim, "An investigation of plasma enhanced combustion," (2006).
20. A. Vincent-Randonnier, S. Larigaldie, P. Magre, and V. Sabelnikov, "Experimental Study of a Methane Diffusion Flame Under Dielectric Barrier Discharge Assistance," to appear in IEEE Transactions (2007).
21. J. A. Bittencourt, Fundamentals of plasma physics 3rd ed., (Springer, 2003).
22. J. Meichsner, "Low Temperature Plasmas," Plasma Physics **670,** 95 (2005).
23. Y. D. Korolev, and I. B. Matveev, "Nonsteady-State Processes in a Plasma Pilot for Ignition and Flame Control," Plasma Science, IEEE Transactions on **34,** 2507-2513 (2006).
24. S. H. Zaidi, E. Stockman, X. Qin, Z. Zhao, S. Macheret, Y. Ju, R. B. Miles, D. J. Sullivan, and J. F. Kline, "Measurements of hydrocarbon flame speed enhancement in high-Q microwave cavity," in *44th AIAA Aerospace Sciences Meeting and Exhibit, AIAA-2006-1217* (2006).
25. J. B. Liu, P. D. Ronney, and M. A. Gundersen, "Premixed flame ignition by transient plasma discharges," Proc. Combust. Inst **29,** 21-26 (2002).
26. W. Kim, M. Godfrey Mungal, and M. A. Cappelli, "The role of in situ reforming in plasma enhanced ultra lean premixed methane/air flames," Combustion and Flame **157,** 374-383 (2009).
27. T. Ombrello, S. H. Won, and Y. Ju, "Lifted Flame Speed Enhancement by Plasma Excitation of Oxygen," in *47th AIAA Aerospace Sciences Meeting and Exhibit, AIAA-2009-689* (2009).
28. E. Mintusov, A. Serdyuchenko, I. Choi, W. R. Lempert, and I. V. Adamovich, "Mechanism of Plasma Assisted Oxidation and Ignition of Ethylene-Air Flows by a Repetitively Pulsed Nanosecond Discharge," in *46th AIAA Aerospace Sciences Meeting and Exhibit, AIAA 2008-1106* (2008).
29. M. Uddi, N. Jiang, E. Mintusov, I. V. Adamovich, and W. R. Lempert, "Atomic Oxygen Measurements in Air and Air/Fuel Nanosecond Pulse Discharges by Two Photon Laser Induced Fluorescence," in *46th AIAA Aerosciences Meeting and Exhibit, AIAA 2008-1110* (Orlando, Fl, 2008).
30. T. Ombrello, and Y. Ju, "Kinetic Ignition Enhancement of H_2 Versus Fuel-Blended Air Diffusion Flames Using Nonequilibrium Plasma," IEEE Tran. Plasma Sci. **36,** 2924-2932 (2008).
31. T. Ombrello, Y. Ju, and A. Fridman, "Kinetic Ignition Enhancement of Diffusion Flames by Nonequilibrium Magnetic Gliding Arc Plasma," AIAA J. **46,** 2424-2433 (2008).
32. X. Rao, K. Hemawan, C. Carter, T. Grotjohn, J. Asmussen, and T. Lee, "Plasma Enhanced Combustion using Microwave Energy Couping in a Re-entrant Cavity Applicator," in *48th Aerospace Sciences Meeting*, AIAA-2010-0651 (Orlando, Fl., 2010).
33. X. Rao, K. Hemawan, C. Carter, I. Wichman, T. Grotjohn, J. Asmussen, and T. Lee, "Combustion Dynamics for Energetically Enhanced Flames using Microwave Energy Coupling," Proc. Combust. Inst. **33,** 3233-3240 (2010).
34. Y. D. Korolev, O. B. Frants, N. V. Landl, V. G. Geyman, and I. B. Matveev, "Glow-to-Spark Transitions in a Plasma System for Ignition and Combustion Control," Plasma Science, IEEE Transactions on **35,** 1651-1657 (2007).
35. Y. D. Korolev, O. B. Frants, N. V. Landl, V. G. Geyman, and I. B. Matveev, "Nonsteady-State Gas-Discharge Processes in Plasmatron for Combustion Sustaining and Hydrocarbon Decomposition," IEEE Transaction on Plasma Science **37,** 586-592 (2009).
36. X. Rao, I. Matveev, and T. Lee, "Nitric Oxide Formation in a Premixed Flame With High-Level Plasma Energy Coupling," IEEE Transaction on Plasma Science **37,** 2303-2313

(2009).
37. X. Rao, I. B. Matveev, and T. Lee, "Nitric Oxide Formation in a Premixed Flame With High-Level Plasma Energy Coupling," IEEE TRANSACTIONS ON PLASMA SCIENCE **37,** 2303 (2009).
38. R. Ono, and T. Oda, "OH radical measurement in a pulsed arc discharge plasma observed by a LIF method," IEEE Transaction on Industry Applications **37,** 709-714 (2001).
39. B. Eliasson, M. Hirth, and U. Kogelschatz, "Ozone synthesis from oxygen in dielectric barrier discharges," J. Phys. D: Appl. Phys. **20,** 1421 (1986).
40. W. Kim, M. Godfrey Mungal, and M. A. Cappelli, "The role of in situ reforming in plasma enhanced ultra lean premixed methane/air flames," Combustion and Flame**,** doi:10.1016/j.combustflame.2009.1006.1016 (2009).
41. K. W. Hemawan, I. S. Wichman, T. Lee, T. A. Grojohn, and J. Asmussen, "Compact Microwave Reentrant Cavity Applicator for Plasma Assisted Combustion," Rev. Sci. Inst. **80,** 053507 (2009).
42. X. Rao, K. Hemawan, I. Wichman, C. Carter, T. Grotjohn, J. Asmussen, and T. Lee, "Combustion dynamics for energetically enhanced flames using direct microwave energy coupling," Proceedings of the Combustion Institute **33,** 3233-3240 (2011).
43. K. Becker, U. Kogelschatz, K. Schoenbach, and R. Barker, Non-equilibrium Air Plasmas at Atmospheric Pressure, (The Institute of Physics, London, 2005).
44. K. Kohse-Hoinghaus, and J. B. Jeffries, Applied Combustion Diagnostics (Taylor & Francis, Inc., New York, 2002).
45. M. Moisan, J. Barbeau, M. Crevier, J. Pelletier, N. Phillip, and B. Saoudi, "Plasma sterilization. Methods and mechanisms," Pure and Applied Chemistry **74,** 349-358 (2002).
46. B. J. Park, D. H. Lee, J. C. Park, I. S. Lee, K. Y. Lee, S. O. Hyun, M. S. Chun, and K. H. Chung, "Sterilization using a microwave-induced argon plasma system at atmospheric pressure," Physics of Plasmas **10,** 4539 (2003).
47. A. Oumghar, J. C. Legrand, A. M. Diamy, and N. Turillon, "Methane Conversion by an Air Microwave Plasma," Plasma Chemistry and Plasma Processing **15,** 87-105 (1995).
48. M. JASIŃSKI, M. DORS, H. NOWAKOWSKA, and J. MIZERACZYK, "Hydrogen Production via Methane Reforming Using Various Microwave Plasma Sources," Chem. Listy **102,** 1332-1337 (2008).
49. J. D. Blahovec Jr, L. A. Bowers, J. W. Luginsland, G. E. Sasser, and J. J. Watrous, "3-D ICEPIC simulations of the relativistic klystron oscillator," Plasma Science, IEEE Transactions on **28,** 821-829 (2002).
50. P. Mardahl, A. Greenwood, T. Murphy, and K. Cartwright, "Parallel performance characteristics of ICEPIC," in *User Group Conference*, (IEEE Computer Society, 2003).
51. A. D. Greenwood, and D. Air Force Research Lab Kirtland Afb Nmdirected Energy, "An ICEPIC Convergence Study Using a Relativistic Magnetron," (2005).
52. J. W. Luginsland, J. J. Watrous, K. L. Cartwright, T. P. Fleming, and M. D. Haworth, "Development of circuit models for extractor components in high power microwave sources," (IEEE, 2006), p. 415.
53. K. Hendricks, J. Watrous, and J. Luginsland, "Experimental and Computational Investigations of a High-Power, Long-Pulse Relativistic Klystron Oscillator," in *Air Force Research Lab Kirtland AFB NM Directed Energy Directorate*, 1 (2006), p. 1121P.